Fungal Genetics and Biology 124 (2019) 73–77

Contents lists available at ScienceDirect

Fungal Genetics and Biology

journal homepage: www.elsevier.com/locate/yfgbi

Nanoscale enrichment of the cytosolic enzyme trichodiene synthase near reorganized endoplasmic reticulum in *Fusarium graminearum*

Marike J. Boenisch[a,1], Ailisa Blum[b,c,1], Karen L. Broz[d], Donald M. Gardiner[b], H. Corby Kistler[d,e,*]

[a] Department of Agronomy and Plant Genetics, University of Minnesota, 411 Borlaug Hall, 1991 Upper Buford Circle, St. Paul, MN 55108, USA
[b] CSIRO Agriculture & Food, Queensland Bioscience Precinct, 306 Carmody Road, St. Lucia, Brisbane, Queensland 4067, Australia
[c] School of Agriculture & Food Sciences, University of Queensland, St. Lucia, Brisbane, Queensland 4072, Australia
[d] USDA ARS Cereal Disease Laboratory, 1551 Lindig Street, St. Paul, MN 55108, USA
[e] Department of Plant Pathology, University of Minnesota, 495 Borlaug Hall, 1991 Upper Buford Circle, St. Paul, MN 55108, USA

ARTICLE INFO

Keywords:
Mycotoxin
Super resolution microscopy
Cytosol

ABSTRACT

Trichothecene mycotoxin synthesis in the phytopathogen *Fusarium graminearum* involves primarily endoplasmic reticulum (ER)-localized enzymes of the mevalonate- and trichothecene biosynthetic pathways. Two exceptions are 3-hydroxy-3-methylglutaryl CoA synthase (Hms1) and trichodiene synthase (Tri5), which are known cytosolic enzymes. Using 3D structured illumination microscopy (3D SIM), GFP-tagged Tri5 and Hms1 were tested for preferential localization in the cytosol proximal to the ER. Tri5 protein was significantly enriched in cytosolic regions within 500 nm of the ER, but Hms1 was not. Spatial organization of enzymes in the cytosol has potential relevance for pathway efficiency and metabolic engineering in fungi and other organisms.

1. Introduction

Fusarium graminearum is a plant pathogenic fungus that contaminates grain crops with sesquiterpene, trichothecene (TRI) mycotoxins that have toxicity to plants and animals (including humans) (Goswami and Kistler, 2004; Rocha et al., 2005). Enzymes in the TRI- and mevalonate pathway (MP) catalyze key steps for TRI biosynthesis (Fig. 1A) and are spatially co-localized at the ER. The MP enzyme HMG-CoA reductase (3-hydroxy-3-methylglutaryl-CoA reductase or Hmr1) catalyzes an important step for synthesis of farnesylpyrophosphate (FPP) and obtains its substrate from HMG-CoA synthase (3-hydroxy-3-methylglutaryl-CoA synthase or Hms1) (Goldstein and Brown, 1990) (Fig. 1A). FPP is substrate for the first reaction of the TRI pathway catalyzed by the enzyme trichodiene synthase (Tri5) (Proctor et al., 1995) in the cytosol (Blum et al., 2016; Boenisch et al., 2017) (Fig. 1A). Downstream reactions of TRI biosynthesis are carried out by other TRI pathway enzymes, such as the cytochrome P450 proteins trichodiene oxygenase (Tri4) and calonectrin oxygenase (Tri1) (Proctor et al., 2018). Under TRI inducing conditions MP enzyme Hmr1 and several TRI pathway proteins, including Tri4, Tri1 (Menke et al., 2013), and Tri14 co-localize in stacks of smooth ER membranes (Fig. 1B) (Boenisch et al., 2017), which are called organized smooth ER (OSER) (Ferrero et al., 2015; Snapp et al., 2003) and were referred to as "toxisomes" of *F. graminearum* previously (Menke et al., 2013). Cytosolic layers (~10 nm wide) between stacked ER membranes may contain the TRI oxygenase- and Hmr1 active sites and, thus may accumulate their reaction products (Boenisch et al., 2017) increasing pathway efficiency and sequestering TRI from targets of inhibition such as ribosomes (de Loubresse et al., 2014) and mitochondria (Bin-Umer et al., 2014) (Fig. 1B). It was recently shown that Tri5 protein is important for OSER formation (Flynn et al., this issue) and OSER formation is required for wild type levels of trichothecene biosynthesis (Tang et al., 2018). In contrast to Tri5, Hms1 is a conserved cytosolic MP protein of the primary metabolism of eukaryotes (Shafqat et al., 2010). Since Tri5 and the MP enzyme Hms1 are localized in the cytosol, we tested whether they may preferentially accumulate near OSER of TRI induced cells, where ER-associated MP and TRI pathway enzymes are localized.

2. Results and discussion

To visualize the distribution of cytosolic enzymes Tri5 and Hms1 surrounding OSER, Tri5-GFP/Tri4-RFP and Hms1-GFP/Tri4-RFP dual-tagged strains were grown in TRI inducing medium and imaged by 3D SIM z series (Fig. 2A and B). Tri5-GFP fluorescence was often pronounced (referred to

Abbreviations: EP, endoplasmic reticulum periphery; FI, fluorescence intensity; 3D SIM, 3D structured illumination microscopy; OSER, organized smooth endoplasmic reticulum; TRI, trichothecene; MP, mevalonate pathway

* Corresponding author at: USDA ARS Cereal Disease Laboratory, 1551 Lindig Street, St. Paul, MN 55108, USA.
E-mail address: hckist@umn.edu (H.C. Kistler).

[1] Authors equally contributed to this work.

https://doi.org/10.1016/j.fgb.2018.12.008
Received 6 August 2018; Received in revised form 16 October 2018; Accepted 18 December 2018
Available online 21 December 2018

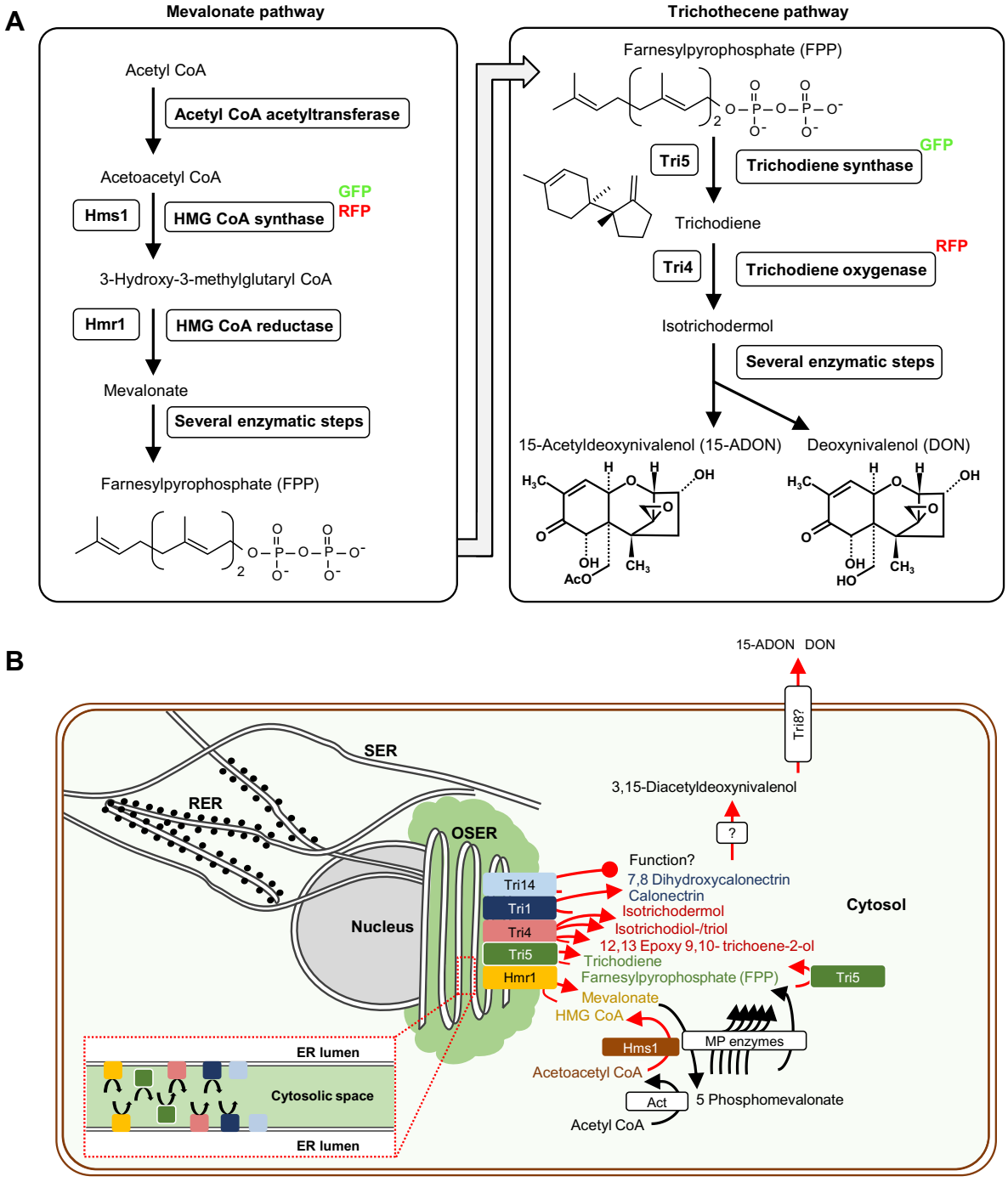

Fig. 1. (A) Fluorescence-tagged enzymes of the mevalonate pathway (MP) and trichothecene pathway (TP) and (B) model of cellular organization of pathway enzymes and reactions under trichothecene (TRI) producing conditions. (A) Two cytosolic enzymes, Hms1 and Tri5, catalyzing early steps of the MP and the TP respectively were tagged at the C-terminus with GFP or RFP. The cytosolic enzyme HMG-CoA synthase (Hms1) provides the substrate 3-hydroxy-3-methylglutaryl CoA (HMG CoA) for HMG-CoA reductase (Hmr1), which catalyzes the synthesis of mevalonate and ultimately farnesyl pyrophosphate (FPP). FPP is substrate for the first step of the TP, which is catalyzed by the trichodiene synthase (Tri5), while subsequent biosynthetic steps for deoxynivalenol (DON) and 15-acetyldeoxynivalenol (15-ADON) are catalyzed by the enzymes trichodiene oxygenase (Tri4), calonectrin oxygenase (Tri1) and other TP enzymes. The cytochrome P450 Tri4 adds the toxic epoxide moiety to the trichodiene backbone and is localized at OSER, along with other subsequent TP proteins. (B) Model of cellular localization of MP and TP proteins (boxes) and their enzymatic reactions (arrows) and metabolites (font color of metabolites match the color of proteins catalyzing the respective reaction) in *F. graminearum* modified from (Boenisch et al., 2017). MP enzyme Hmr1 and TP proteins Tri4, Tri1, and Tri14 co-localize at OSER upon TRI induction. OSER are stacks of smooth ER membranes, separated by a ~10 nm cytosolic space. This study indicates an enrichment of Tri5 surrounding the OSER periphery (green cloud) and in cytosolic spaces within OSER (green background in detail – red dashed box), which may promote pathway efficiency and sequestration of toxic intermediates from targets of TRI inhibition. ? = Unknown protein, protein function (Tri14), or protein localization (Tri8). Abbreviations in panel B: OSER organized smooth endoplasmic reticulum, RER rough endoplasmic reticulum, SER smooth endoplasmic reticulum. Note that proportions in B do not represent authentic scales. (For interpretation of the references to color in this figure legend, the reader is referred to the web version of this article.)

here as "clusters") surrounding Tri4-RFP labeled OSER (Fig. 2, left panels) and often also co-localized with Tri4-RFP fluorescence within OSER (Fig. 2A, right panels). In contrast to Tri5, the cytosolic MP enzyme Hms1-GFP usually appeared evenly distributed throughout the cytosol (Fig. 2B). Clusters of cytosolic Tri5 near OSER, compared to the rather homogenously distributed Hms1 in the cytosol, were confirmed using a Tri5-GFP/Hms1-RFP strain under identical growth conditions for 3D SIM z-stack imaging (Fig. 2C). For comparison, conventional epifluorescence micrographs of strains Tri5-GFP/Tri4-RFP (Fig. S1), Hms1-GFP/Tri4-RFP (Fig. S2), and Hms1-RFP/Tri5-GFP (Fig. S3) grown in TRI inducing medium and minimal medium (without TRI induction) are provided in Supplementary Figs. S1–S3. Clusters of Tri5-GFP surrounding the periphery of OSER are

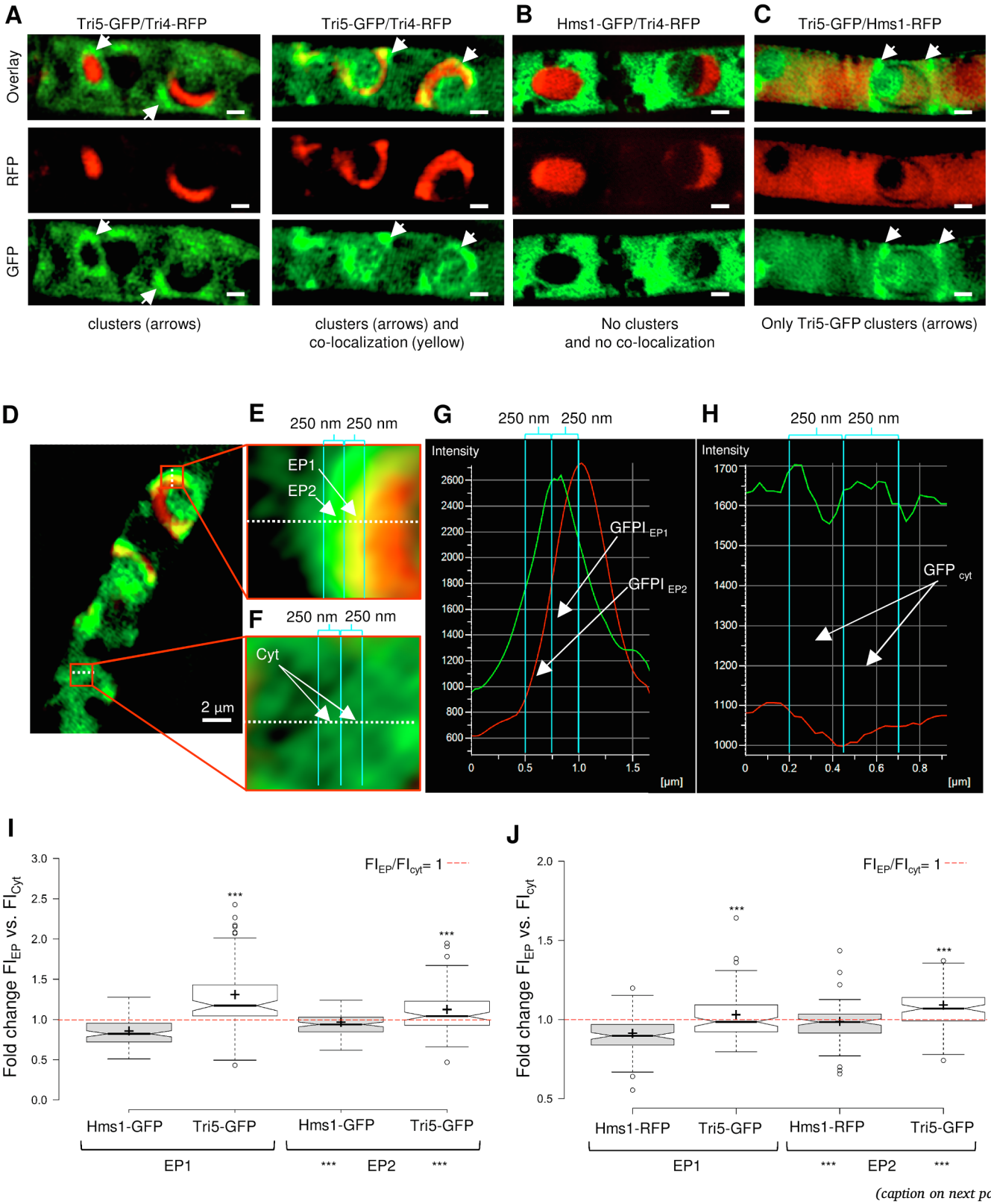

(caption on next page)

Fig. 2. Super resolution microscopy of cytosolic Tri5 and Hms1. A–C 3D SIM z-stack images of dual fluorescently labeled strains (A) Tri5-GFP/Tri4-RFP, (B) Hms1-GFP/Tri4-RFP and (C) Tri5-GFP/Hms1-RFP grown in TRI inducing medium for 48 h. (A) Left panels: Clusters (arrows) of Tri5-GFP (green) surrounding Tri4-RFP labeled OSER (red) and, right panels: Clusters (arrows) of Tri5-GFP (green) partially co-localize (yellow) with Tri4-RFP labeled OSER (red) in a Tri5-GFP/Tri4-RFP strain. Clusters or co-localization were usually not observed with Hms1-GFP of strain Hms1-GFP/Tri4-RFP (B) nor with Hms1-RFP in a Tri5-GFP/Hms1-RFP strain, although clusters (arrows) of Tri5-GFP surrounding non-fluorescent OSERs were observed in strain Tri5-GFP/Hms1-RFP (C). Scale bars = 1 µm. D–J Quantification of Tri5 and Hms1 fluorescence at OSER. D OSER (red dashed box, detailed in E) and a cytosolic region distal from the OSER (red dashed box, detailed in F) were identified in z-stacks of hyphae from n = 91 features. E-H Fluorescence intensity (FI) in two 250 nm regions at the ER periphery (EP1 and EP2 in E and G) and regions distal to OSER (Cyt in F and H) were determined by intensity profiles (G and H). I and J Boxplots of mean fold change differences in fluorescence intensity (FI) of Tri5 and Hms1 tagged protein in EP1 and EP2 relative to Cyt for strains Tri5-GFP/Tri4-RFP and Hms1-GFP/Tri4-RFP (I) and Tri5-GFP/Hms1-RFP (J). Notched boxes show the interquartile range (IQR) of the middle 50% of the data, crosses show mean values, circles outliers of the data sets, and the whiskers indicate data points < 1.5 × IQR from the first or third quartile according to Tukey test. Non-overlapping notches (95% confidence intervals (+/1.58 × IQR/sqrt(n))) between Tri5 and Hms1 in EP1 and EP2 indicate that the respective medians (bold band) differ significantly. Bars = standard deviation, n = 91, *** $p < 0.005$, two-tailed Student's t-test. (For interpretation of the references to color in this figure legend, the reader is referred to the web version of this article.)

illustrated by 3D surface rendering (Video 1). Video 1 visualizes the highest Tri5-GFP fluorescence intensities within the z-stack of an OSER, representatively for strain Tri5-GFP/Tri4-RFP. Optical sectioning along the z dimension of a 3D reconstructed OSER demonstrates Tri5-GFP fluorescence not only at the OSER periphery, but also within OSER, as indicated by yellow signals, resulting from overlapping Tri5-GFP and Tri4-RFP fluorescence (Video 1, Supplementary Fig. S4A). Similar observations were not common with strain Hms1-GFP/Tri4-RFP (Supplementary Fig. S4B).

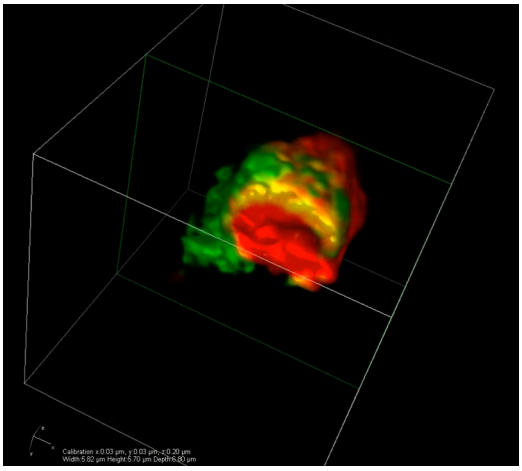

Video 1. 3D SIM volume rendering of an OSER of a Tri5-GFP/Tri4-RFP strain. Optical sectioning through 3D reconstructed OSER shows Tri5-GFP fluorescence surrounding the cytosol-facing surface of Tri4-RFP labeled OSER (green fluorescence). Tri5-GFP fluorescence inside OSER is indicated by yellow fluorescence, resulting from the overlay of RFP and GFP channels (See also Supplementary Fig. S4A). Scale bar = 1 µm.

In order to study clustering of Tri5 and Hms1 near OSER, only mature fungal cells, which showed at least one distinct OSER, were imaged by 3D SIM. To quantify clustering of Tri5 and Hms1 near OSER, we measured fluorescence intensity (FI) of Tri5-GFP, Hms1-GFP, and Hms1-RFP at the periphery of OSER (n = 91 per strain) in the strains Tri5-GFP/Tri4-RFP, Tri5-GFP/Hms1-RFP, and Hms1-GFP/Tri4-RFP. Cytosolic FI of GFP or RFP tagged Tri5 and Hms1 was determined within 500 nm of the OSER periphery and compared with FI in cytosolic regions distal to OSER in the same cell (Fig. 2D–H). For each measurement, OSER proximal and distal cytosolic regions (red dashed boxes in Fig. 2D) were identified in z-stack images (Fig. 2D). FI in two 250 nm regions at the ER periphery (EP1 and EP2 in Fig. 2E) and in a 250 nm distal region (Cyt in Fig. 2F) were measured in the same optical section of the z-stack, using intensity profiles (Fig. 2G and H). FI values in EP1 and EP2 for Tri5-GFP, Hms1-GFP, and Hms1-RFP were taken from optical sections showing the maximum FI along the z-stack of an OSER (n = 91). Mean FI_{EP1} and FI_{EP2} were normalized to the corresponding FI_{Cyt} value, which represents the mean of ten measurements along a 250 nm transect. In this manner, the signal ratios of FI_{EP1} and FI_{EP2} to FI_{Cyt} were determined for Tri5 and Hms1. Mean FI_{EP1} and FI_{EP2} forTri5-GFP were, respectively, 29% and 10% higher compared to FI_{Cyt} (Fig. 2I). In contrast, mean FI_{EP1} and FI_{EP2} for Hms1-GFP were 17% and 6% lower compared to FI_{Cyt} (Fig. 2I). Mean differences between Tri5 and Hms1 were highly significant in EP1 ($p < 10^{-18}$) and EP2 ($p < 10^{-6}$). Furthermore, FI of Tri5-GFP in EP1 compared to EP2 was significantly higher ($p < 10^{-3}$), indicating greater protein accumulation toward the OSER. The opposite was observed with Hms1-GFP, where FI_{EP1} is significantly lower compared to FI_{EP2} ($p < 10^{-6}$) (Fig. 2I). Repeating the experiments with a Tri5-GFP/Hms1-RFP strain confirmed differential clustering at OSER between Tri5-GFP and Hms1-RFP in EP1 ($p < 10^{-8}$) and EP2 ($p < 10^{-13}$) and between EP1 and EP2 for Tri5-GFP ($p < 10^{-10}$) and Hms1-RFP ($p < 10^{-8}$) (Fig. 2J). This demonstrates that differences between Tri5 and Hms1 in clustering at OSER, in strains dual-tagged with Tri4-RFP, are not due to presence of Tri4-RFP, since differences were also seen in the Tri5-GFP/Hms1-RFP strain in the absence of Tri4-RFP. Differences in fluorescence patterns also were not caused by measurements from different cells since FI measurements of Tri5 and Hms1 in the Tri5-GFP/Hms1-RFP strain were from the same cell. Due to the lack of a fluorescent ER marker in the Tri5-GFP/Hms1-RFP strain, borders for EP1 and EP2 were defined by the non-fluorescent crescent silhouette of OSER membranes. Borders for EP1 and EP2, thus may have been biased towards the OSER, thereby reducing the FI of EP1 and EP2 for Tri5 and Hms1 compared to results from strains with the Tri4-RFP ER marker. Differences in both arithmetic mean and median FI values further support that Tri5 is enriched in both EPI and EP2, compared to Hms1 (Fig. 2I and J).

The reason why cytosolic Hms1 was not significantly enriched near OSER remains unknown. Future studies will be needed to determine, whether clusters of Hms1 might be detected by SIM at other time points during TRI induction or under different growth conditions. We speculate that spatial sequestration of Tri5 could be useful to prevent self-inhibition by product toxification, while metabolites synthesized by Hms1 and MP enzymes are non-toxic, essential metabolites, which may not have necessitated evolution of specialized sequestration. Interestingly, many clustering cytosolic proteins identified in *Saccharomyces cerevisiae* are involved in intermediary metabolism or stress responses rather than primary metabolism (Narayanaswamy et al., 2009).

Spatial enrichment of cytosolic Tri5-GFP near OSER was not resolved with conventional fluorescence microscopy previously (Blum et al., 2016; Boenisch et al., 2017) or in this study (Supplementary Fig. S1, left panels). Our 3D SIM results however demonstrate that, although the trichodiene synthase Tri5 is a soluble protein, it is enriched in the vicinity of the OSER, likely even within the cytosol containing layers of smooth ER cisternae (Video 1) (Boenisch et al., 2017). As Tri5 is important for OSER formation (Flynn et al., this issue), its position vis-à-vis the OSER may stabilize adjacent sheets of ER cisternae and bring Tri5 together with the ER membrane-bound enzymes of the TRI pathway. In doing so, Tri5 may increase pathway efficiency and allow sequestering of toxic pathway intermediates from the targets of TRI inhibition in the fungal cell. Also known as Fusarium "toxisomes,"

OSER are being targeted to identify agrichemicals that specifically reduce mycotoxin contamination by preventing OSER formation (Tang et al., 2018). A detailed knowledge of the spatial organization of enzymatic pathways in the cell may be critical for understanding metabolic dynamics in living organisms and may have benefits for engineering metabolic pathways.

3. Methods

3.1. Fungal growth and reporter strains

All strains were created in *F. graminearum* wild type strain PH-1 (NRRL 31084) and induced to produce TRI by published methods (Boenisch et al., 2017). Tri5 and Hms1 were tagged at the C-terminus in their native genomic locus with GFP or RFP similar to strains Tri5-GFP and Tri5-GFP/Tri4 RFP published previously (Boenisch et al., 2017). Reporter strains Hms1-GFP and Hms1-RFP were generated using a fusion PCR method (Boenisch et al., 2017). Hms1 protein was tagged with GFP by replacing the stop codon of HMS1 with the *GFP::hph::loxP* fragment from vector *pGFP::hph::loxP* (Honda and Selker, 2009). For RFP tagging, the *RFP::nat1* fragment of pAL12-Lifeact vector (Fungal Genetics Stock Center, Kansas City) (Lichius and Read, 2010) was used. Selection and verification of transformants were performed as described previously (Boenisch et al., 2017) with appropriate primers. The dual fluorescently labeled strain Tri5-GFP/Hms1-RFP was generated by sexual crossing of single fluorescently labeled strains as described earlier (Boenisch et al., 2017), using Tri5-GFP and Hms1-RFP strains.

3.2. Super resolution microscopy

Hyphae from TRI-induced cultures were washed, mounted on glass slides and covered with high precision 18 × 18 mm glass coverslips for super resolution microscopy (Boenisch et al., 2017). The Nikon 3D-SIM system with an inverted Nikon Ti-E microscope and a Nikon structured illumination system was used with an Apo TIRF 100× oil objective. Laser light at 561 nm (excitation) and 600 nm (emission) was used for RFP detection, while laser excitation of 488 nm and emission at 525 nm was used for GFP. Z-stacks in 0.2 µm steps were acquired using 3D SIM mode with a MCL Nano Piezo Z Drive. Images with 1024 × 1024 pixel in x/y and 0.03 µm/pixel calibration were taken with an Andor DU-897 X-8444 camera. The Nikon NIS Elements AR software 4.20.02 was used for image acquisition and SIM reconstruction. 3D rendering was done with the shaded surface feature of the Nikon NIS elements AR software 4.30.01.

Conflict of interest

None.

Acknowledgements

We thank Mark Sanders and Guillermo Marques at the University of Minnesota Imaging Centers for technical support during super resolution microscopy. This work was funded by award 2018-67013-28512 from the Agriculture and Food Research Initiative of the National Institute of Food and Agriculture, United States Department of Agriculture. A.B. was funded by a University of Queensland Graduate School International Travel Award and a School of Agriculture and Food Sciences travel scholarship.

Appendix A. Supplementary material

Supplementary data to this article can be found online at https://doi.org/10.1016/j.fgb.2018.12.008.

References

Bin-Umer, M.A., et al., 2014. Elimination of damaged mitochondria through mitophagy reduces mitochondrial oxidative stress and increases tolerance to trichothecenes. Proc. Natl. Acad. Sci. 111, 11798–11803. https://doi.org/10.1073/pnas.1403145111.

Blum, A., et al., 2016. High-throughput FACS-based mutant screen identifies a gain-of-function allele of the *Fusarium graminearum* adenylyl cyclase causing deoxynivalenol over-production. Fungal Genet. Biol. 90, 1–11. https://doi.org/10.1016/j.fgb.2016.02.005.

Boenisch, M.J., et al., 2017. Structural reorganization of the fungal endoplasmic reticulum upon induction of mycotoxin biosynthesis. Sci. Rep. 7, 44296. https://doi.org/10.1038/srep44296.

de Loubresse, N.G., et al., 2014. Structural basis for the inhibition of the eukaryotic ribosome. Nature 513, 517–522. https://doi.org/10.1038/nature13737.

Ferrero, S., et al., 2015. Proliferation and morphogenesis of the endoplasmic reticulum driven by the membrane domain of 3-hydroxy-3-methylglutaryl coenzyme A reductase in plant cells. Plant Physiol. 168, 899–914. https://doi.org/10.1104/pp.15.00597.

Flynn, C.M., et al., 2018;al., this issue. Expression of the *Fusarium graminearum* terpenome and involvement of the endoplasmic reticulum-derived toxisome. Fungal Genet. Biol (this issue).

Goldstein, J.L., Brown, M.S., 1990. Regulation of the mevalonate pathway. Nature 343, 425–430. https://doi.org/10.1038/343425a0.

Goswami, R.S., Kistler, H.C., 2004. Heading for disaster: *Fusarium graminearum* on cereal crops. Mol. Plant Pathol. 5, 515–525. https://doi.org/10.1111/j.1364-3703.2004.00252.x.

Honda, S., Selker, E.U., 2009. Tools for fungal proteomics: multifunctional *Neurospora* vectors for gene replacement, protein expression and protein purification. Genetics 182, 11–23. https://doi.org/10.1534/genetics.108.098707.

Lichius, A., Read, N.D., 2010. A versatile set of Lifeact-RFP expression plasmids for live-cell imaging of F-actin in filamentous fungi. Fungal Genet. Rep. 57, 8–14. https://doi.org/10.4148/1941-4765.1070.

Menke, J., et al., 2013. Cellular development associated with induced mycotoxin synthesis in the filamentous fungus *Fusarium graminearum*. PLoS One 8, e63077. https://doi.org/10.1371/journal.pone.0063077.

Narayanaswamy, R., et al., 2009. Widespread reorganization of metabolic enzymes into reversible assemblies upon nutrient starvation. Proc. Natl. Acad. Sci. 106, 10147–10152. https://doi.org/10.1073/pnas.0812771106.

Proctor, R.H., et al., 1995. Reduced virulence of *Gibberella zeae* caused by disruption of a trichthecine toxin biosynthetic gene. Mol. Plant Microbe Interact. 8, 593–601. https://doi.org/10.1094/MPMI-8-0593.

Proctor, R.H., et al., 2018. Evolution of structural diversity of trichothecenes, a family of toxins produced by plant pathogenic and entomopathogenic fungi. PLoS Pathog. 14, e1006946. https://doi.org/10.1371/journal.ppat.1006946.

Rocha, O., et al., 2005. Effects of trichothecene mycotoxins on eukaryotic cells: a review. Food Addit. Contam. 22, 369–378. https://doi.org/10.1080/02652030500058403.

Shafqat, N., et al., 2010. Crystal structures of human HMG-CoA synthase isoforms provide insights into inherited ketogenesis disorders and inhibitor design. J. Mol. Biol. 398, 497–506. https://doi.org/10.1016/j.jmb.2010.03.034.

Snapp, E.L., et al., 2003. Formation of stacked ER cisternae by low affinity protein interactions. J. Cell Biol. 163, 257–269. https://doi.org/10.1083/jcb.200306020.

Tang, G., et al., 2018. The fungal myosin I is essential for *Fusarium* toxisome formation. PLoS Pathog. 14, e1006827. https://doi.org/10.1371/journal.ppat.1006827.